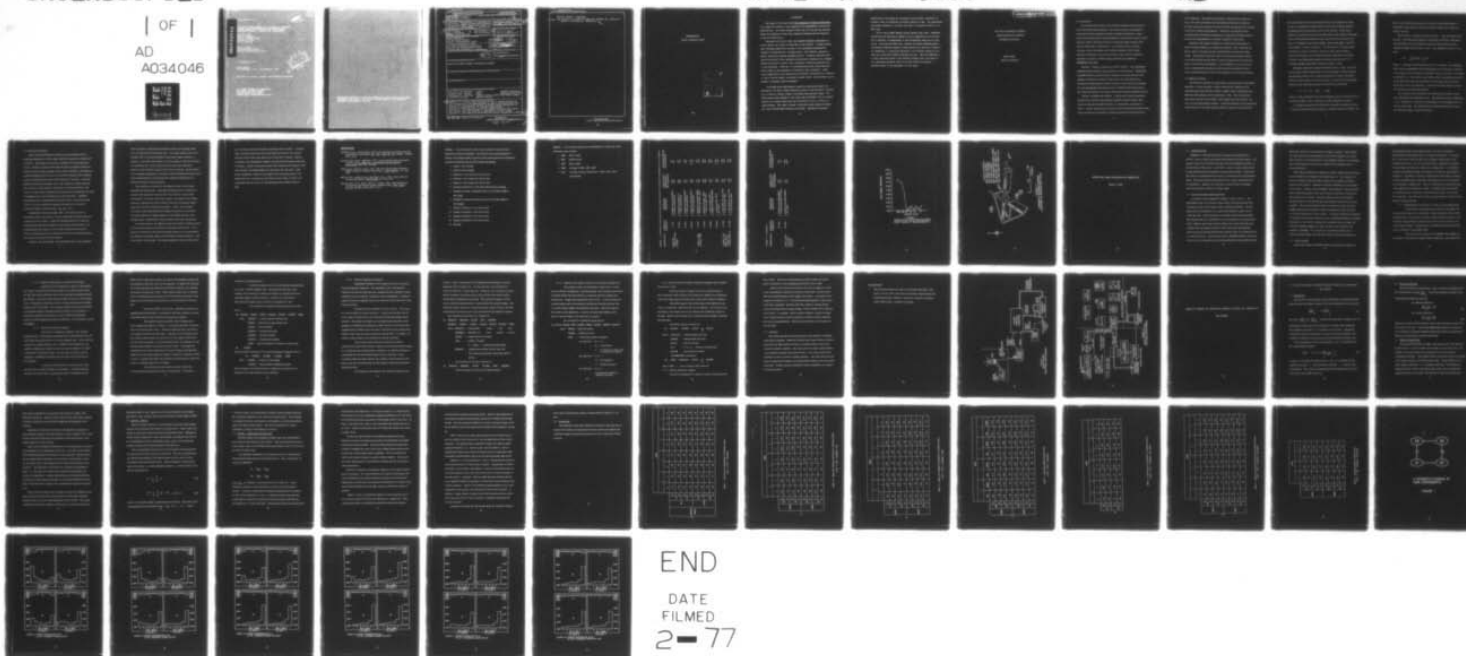


AD-A034 046

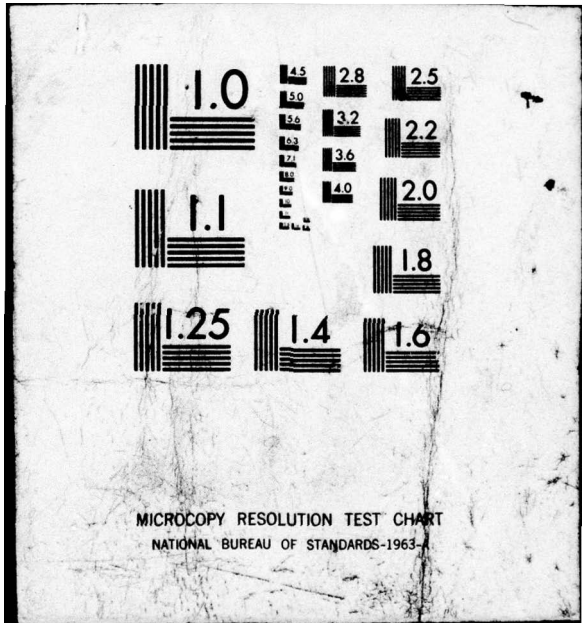
REGIS COLL WESTON MASS  
VISIBILITY MEASUREMENTS FOR PROBABILITY FORECASTS; MCIDAS SYSTEM--ETC(U)  
SEP 76 J M WARD, M R HERMANN, L BURKE F19628-75-C-0074  
AFGL-TR-76-0250 NL

UNCLASSIFIED

| OF |  
AD  
A034046  
DATE  
FILMED



END  
DATE  
FILMED  
2-77



MICROCOPY RESOLUTION TEST CHART  
NATIONAL BUREAU OF STANDARDS-1963-A

ADA034046

AFGL-TA-76-0250

VISIBILITY MEASUREMENTS FOR PROBABILITY FORECASTS  
MCIDAS SYSTEM CONFIGURATION AND CAPABILITIES  
RADIATIVE CHANGE OF SURFACE AIR TEMPERATURE

Joan M. Ward  
Mary R. Hermann  
Sister Leonarda Burke  
Harold J. Pratt  
Roy M. Glasser

Regis College  
235 Wellesley Street  
Weston, Massachusetts 02193

30 September 1976

Final Report  
(20 September 1974 - 30 September 1976)

Approved for public release; distribution unlimited

AIR FORCE GEOPHYSICS LABORATORY  
AIR FORCE SYSTEMS COMMAND  
UNITED STATES AIR FORCE  
HANSCOM AFB, MASSACHUSETTS 01731

DDC  
RECEIVED  
JAN 6 1977  
8

1493

Qualified requestors may obtain additional copies from the Defense Documentation Center. All others should apply to the National Technical Information Service.

<b>19 REPORT DOCUMENTATION PAGE</b>		<b>READ INSTRUCTIONS BEFORE COMPLETING FORM</b>
1. REPORT NUMBER <b>18 AFGL-TR-76-0250</b>	2. GOVT ACCESSION NO.	3. RECIPIENT'S CATALOG NUMBER <b>9</b>
6. TITLE (and Subtitle) <b>VISIBILITY MEASUREMENTS FOR PROBABILITY FORECASTS; MCIDAS SYSTEM CONFIGURATION AND CAPABILITIES; RADIATIVE CHANGE OF SURFACE AIR TEMPERATURE.</b>		5. TYPE OF REPORT & PERIOD COVERED <b>Scientific Report Final 20 Sep 74-30 Sep 76</b>
7. AUTHOR(s) <b>Joan M./Ward, Harold/Pratt Mary R./Hermann, Roy M./Glasser Leonarda/Burke</b>		8. CONTRACT OR GRANT NUMBER(s) <b>F19628-75-C-0074</b>
9. PERFORMING ORGANIZATION NAME AND ADDRESS <b>Regis College 235 Wellesley Street Weston, Massachusetts 02193</b>		10. PROGRAM ELEMENT, PROJECT, TASK AREA & WORK UNIT NUMBERS <b>62101 F 8604001</b>
11. CONTROLLING OFFICE NAME AND ADDRESS <b>Air Force Geophysics Laboratory Hanscom AFB, Massachusetts 01731 Contract Monitor/Peter A. Giorgio/LY</b>		12. REPORT DATE <b>30 Sep 76</b>
14. MONITORING AGENCY NAME & ADDRESS (if different from Controlling Office)		13. NUMBER OF PAGES <b>56</b>
16. DISTRIBUTION STATEMENT (of this Report)  Approved for public release; distribution unlimited		15. SECURITY CLASS. (of this report) <b>Unclassified</b>
		15a. DECLASSIFICATION/DOWNGRADING SCHEDULE
17. DISTRIBUTION STATEMENT (of the abstract entered in Block 20, if different from Report)		
18. SUPPLEMENTARY NOTES		
19. KEY WORDS (Continue on reverse side if necessary and identify by block number)		
extinction coefficient      raster      forward difference Allard's Law (night)      pixel      backward difference Koschmieder's Law (day)      forward scatter meter wave-number space stretched raw data      2400 Hz carrier		
20. ABSTRACT (Continue on reverse side if necessary and identify by block number)		
Section 1: A pilot study was carried out to assess effects of time averaging of raw measurements on short-time predictability, as part of a development program directed toward automation of short-term forecasts and of airfield observations. Section 2: The capabilities of the general basic McIDAS system are studied with the purpose of adapting it to AFGL usage. Section 3: Six tables of pertinent statistical parameters present		

ne pag  
mt

Unclassified

SECURITY CLASSIFICATION OF THIS PAGE(When Data Entered)

Block 20, Section 3 (continued)

cont → results of a study of numerical schemes for radiative  
change in surface air temperature. ↖

Unclassified

SECURITY CLASSIFICATION OF THIS PAGE(When Data Entered)

INTRODUCTION

Sister Leonarda Burke

APPROVAL FOR		
NTIS	DATE	<input checked="" type="checkbox"/>
DIS	DATE	<input type="checkbox"/>
UNCLASSIFIED		<input type="checkbox"/>
JUSTIFICATION		
BY		
DISTRIBUTION/AVAILABILITY STATEMENTS		
DATE		
A		

## Introduction

The purpose of the pilot study Time Averaging of Visibility Measurement is to assess the effects of time averaging of raw measurements on short-time predictability. The larger program of which this is to be part was directed toward the automation of short-term visibility forecasts and the automation of airfield observations.

Throughout the initial study, the automated mesoscale measurements of surface weather are limited to those made on the airfield. A forward scatter meter developed commercially was used in the experimental program which included all occasions over a two-year period. More recently, analyses of spatial variability produced remarkable results. Screening regression techniques and multiple linear regression equations were developed, and a computer program was written to select, after correlation, effective predictors with a given predictand. Ruled out in a screening process were those predictors which yielded no new information as revealed by high correlation. Proper initial application of the unconditional probability distribution as a function of time of day and season, can provide on-going results. Diurnal effects can be managed in stochastic model development.

The McIDAS system (Man-Computer Interactive Data Access System) was developed at the Space Sciences Engineering Center at the University of Wisconsin, to archive, process, analyze, and display meteorological images. The McIDAS applications programs in this report show the McIDAS to be an extremely powerful and flexible system that can be modified for use in a variety of image problems. This report includes a functional system diagram of McIDAS and a more detailed block diagram of the system. Typifying the multiple

capabilities of the system are calculation of wind vectors, generation of animation loops, and scheduled unattended ingestion of data. The improvements and changes discussed in the report were made in the system to adapt it for AFGL usage.

The Air Force Global Weather Central Boundary Layer Model, (AFGWC-BLM) assumes that the time rate of change of the air temperature at the surface, due to radiation, is proportional to the corresponding change due to climatology. This study has shown that, although the current AFGWC-BLM employs the backward difference formula for approximating the time-rate of change of air temperature, no significant difference in the forecast accuracy of the model was evident when forward difference was used. Since the AFGWC-BLM is a highly complicated model of the planetary boundary layer, the method of twin experiments presented itself as the most effective technique. A detailed account of the experiment is in the report.

**The Time Averaging of Visibility  
Measurements for Conditional  
Probability Forecasts**

**Joan M. Ward**

**Mary R. Hermann**

## 1.1 Introduction

The representative nature of the visibility estimates that are derived from instrumental measurements is one of the important considerations associated with the automation of aviation weather observations. Rapid advances have been made in the development of point visibility sensors which measure scatter coefficients and also in short path length systems which measure atmospheric transmission. In reasonably uniform visibility situations, these instruments yield reliable estimates of the average extinction coefficient in the local area which in turn convert to effective estimates of observer visibility through Allard's Law (night) and Koschmieder's Law (day).

However, visibility conditions are seldom uniform. Fog components characteristically exhibit large variability in space and time. Although the automated sensors provide excellent capability to monitor the local time changes in extinction coefficient continuously, the measurements are influenced by high frequency spatial fluctuations which tend to be smoothed by vision through the atmosphere and thus constitute measurement noise. The lower the visibility, the smaller the effective spatial smoothing interval.

Figure 1 illustrates the problem. It shows the correlation spectrum between point visibility measurements obtained at Hanscom AFB, Mass., observing sites ERY and NRY (see Fig. 2), which have a separation of 1240 m. Shallow ground fog occurrences were excluded from the data sample, which consisted of 32 episodes of advection fog observed during 1972 and

1973 at Hanscom. The observed fluctuations, with periods less than one hour, show little correlation over the distance between the two stations, yet these small scale variations account for about one-half the total variance of the point visibility measurements. Therefore, key questions arise concerning the most effective techniques for using point visibility observations for the representation of visibility conditions on the airfield.

Analyses of the spatial variability of visibility have been made in a series of recent studies (e. g. George and Lefkowitz, 1972, Chisholm and Kruse, 1974), which help provide a rational basis for observing system design. The purpose of this pilot study is to assess yet another aspect of the problem dealing with the effects of time averaging of the raw measurements on short-term predictability. The investigation was carried out as part of a development program directed toward the automation of short-term visibility forecasts as well as the automation of airfield observations.

## 1.2 Method of Analysis

The data base consists of a long series of measurements of atmospheric extinction, or more precisely, scatter coefficient ( $b$ ), gathered by the automated mesoscale network of surface weather stations established near Hanscom AFB, (Hering, Brown and Muench, 1972). The measurements were made with the forward scatter meter (FSM) developed by EG+G, Inc., for use in the experimental program. A detailed summary of the performance characteristics of the FSM is given by Muench, Moroz and Jacobs (1974).

The measurement precision as determined from rms differences in side by side (3 m separation) measurements in restricted visibility conditions (excluding shallow ground fog) is four to seven percent. In this study, attention is restricted to the measurements made on the airfield at Hanscom. Three observing sites along the runway, each elevated 4 m above ground level, are designated west runway (WRY), north runway (NRY), and east runway (ERY), as shown in Figure 2. For this analysis, the data sample included all occasions, (N=4162), during a two year period ending in January 1975 when the area averaged extinction coefficient as calculated from the 1-min FSM measurements at the three sites was  $2 \times 10^{-3} \text{ m}^{-1}$  or greater (daytime equivalent visibility less than 1.5 km).

Screening regression techniques (Glahn and Lowry, 1972), were used to explore the relative effectiveness of various methods of time averaging. An immediate objective was to select the best form of input to stochastic models for short-range (0-3 hours) forecasts of runway visual range (RVR). Multiple linear regression equations were developed of the form,

$$\hat{y} = a_0 + a_1 + a_2 x_2 \dots a_K x_K$$

where  $\hat{y}$  is the estimated value of the predictand, the  $x$ 's are the predictors as listed in Tables 1 and 2, and the  $a_i$ 's are the regression constants.

A computer program was written which performs a screening process to select the variable having the highest correlation with the predictand, and

then to select additional predictors in the order of their effectiveness, in combination with predictors previously selected, which act to reduce the residual variance.

The predictors screened are listed in Table 1. They are derived from the basic 1-min FSM measurements of atmospheric extinction coefficients. The parameters are self explanatory with the possible exception of the weighted averages listed as items 7 and 8. The weighting function is of the form,

$$\bar{X} = \frac{\sum_{t=0}^{\infty} K^t X(t)}{\sum_{t=0}^{\infty} K^t}$$

where  $t$  is the age of the observation and  $K$  is a constant. The weighting factors decay exponentially with increasing age of the observation, reducing to 10 percent in three minutes for parameter 7 and to 10 percent in 10 minutes for parameter 8. The predictor set consists of the 12 parameters calculated for the three observing sites and the two area averages shown in Table 2 which yield a total of 60 predictors. The local time with respect to sunrise was included as an additional predictor.

For purposes of this evaluation, the predictand and predictor values were transformed into logarithmic form. The standard errors of regression,  $\Delta \ln b$ , represent, to a good first approximation, the percentage errors in runway visual range. The resultant error distribution tends to be normal over the broad range of observed visibility.

### 1.3 Discussion of Results

Some of the results that are relevant to the development of fully automated techniques for short-range visibility forecasts are summarized in Table 3. The program produced four predictors for each predictand chosen. However, because of the relatively high correlation between the alternate forms of time-averaged values used as predictors, the addition of predictors beyond the first one or two that were selected by the screening process contributed little to the further reduction of variance. Directing attention to the first predictand, the 1-min average at a single observing site, the first or best predictor selected for all forecast intervals from 5 min. to 1 hour was the weighted time average with an exponential decrease in weighting factor with increasing age of the observation. Additional experimentation has indicated that exponential decay to 10 percent at age 10-min is close to optimum for general application to all classes of restricted visibility conditions (rain, fog, snow, etc.).

Unexpectedly, the area average, RWY, was selected only as a secondary predictor and served to further reduce the residual variance by a mere one to two percent. It should be emphasized that for single site predictions the regression estimates based simply upon the latest 1-min average at that site compare very favorably with the results shown in Table 3; the standard errors of estimate for the various forecast intervals are larger by only three to seven percent.

Similarly, the area average, with exponential decay of the weighting

factor with time, yields the best estimates of the 3-site average values for 5-min and 15-min forecast intervals. For longer periods, the 1-min average of the 3-site measurements produced the largest reduction of variance. Local time with respect to sunrise appears as the second predictor selected for the 1-hour forecast period in this mean regression analysis, which is based on data from all hours of the day. Diurnal effects can be managed competently in stochastic model development through proper initial representation of the unconditional probability distribution as a function of the time of day and season.

The reductions in variance for the single site and 3-site average estimates are quite similar. Note that the standard error of estimate of runway visual range even over the short 5-min interval is quite large (45 percent). In common with earlier studies, the addition of the change predictors reflecting the recent visibility trend does not enhance significantly the short-term regression estimates. In fact, the calculated correlation coefficients between the changes observed over consecutive 15-minute periods are slightly negative for both single site and 3-site average values, reflecting the strong influence of the noise components.

In current practice, the highest and the lowest values of RVR observed over the past 10 minutes are encoded for long line transmission. It is of interest to determine if the observed extreme values are as representative for estimates of extreme values in the near term as other predictors, such as the latest 1-min average. The answer appears to be yes for the period

up to +15 min as shown for the third predictand listed in Table 3. Of those listed, the best predictor for the lowest RVR over the first two forecast intervals is the lowest value observed over the past 10 minutes. Beyond 15 minutes, the exponentially weighted averages yield the largest reductions of variance. Similar results (not shown) were obtained in the analysis of the other extreme, the highest RVR to be expected in the near term. After proper adjustment is made for the length of the forecasting interval, the standard errors of estimate for the extreme values shown in Table 3 are comparable with the errors for estimating the most probable values of RVR.

## REFERENCES

- Chisholm, D. A., and H. Kruse, 1974: The variability of airfield visibility: a preliminary assessment, Env. Res. Paper No. 462, AFCRL, January 1974, 30 pp.
- George, D. H. and M. Lefkowitz, 1972: A new concept: sensor equivalent visibility, Proc. AMS Conf. on Aerospace and Aeronautical Meteorology, May 1972, 243-250.
- Glahn, H. R., and D. A. Lowry, 1972: The use of Model Output Statistics (MOS) in objective weather forecasting, J. Appl. Meteor., 11, 1203-1211.
- Hering, W. S., Muench, H. S., and Brown, H. A. 1972: Mesoscale forecasting experiments, Bulletin AMS, 53, 1180-1183.
- Muench, H. S., E. Y. Moroz, and L. P. Jacobs, 1974: Development and calibration of the forward scatter visibility meter, Instr. Paper No. 217, AFCRL, March 1974, 37 pp.

**TABLE 1. List of predictors which were screened to produce linear regression prediction equations. All predictors are representations of Runway Visual Range (RVR) as given by point measurements of atmospheric extinction coefficient with forward scatter instruments.**

1. Latest 1-min average
2. Latest 10-min average
3. Maximum 1-min value over last 10-min
4. Minimum 1-min value over last 10-min
5. Range of 1-min values over last 10-min
6. Standard deviation of 1-min values about 10-min average
7. Weighted average, exponential decay to 10 percent weight at age 3-min
8. Weighted average exponential decay to 10 percent weight at age 10-min
9. Change in predictor 1 over last 10 min
10. Change in predictor 2 over last 10 min
11. Change in predictor 7 over last 10 min
12. Change in predictor 8 over last 10 min
13. Sun time

**TABLE 2. List of observing sites and combinations of sites from which predictors were screened.**

1. **WRY**    **West runway**
2. **NRY**    **North runway**
3. **ERY**    **East runway**
4. **BED**    **Average of WRY, NRY, ERY**
5. **RWY**    **Average of natural logarithms of WRY, NRY, ERY  
observations.**

TABLE 3. Predictors selected and the associated reduction of variance and standard error of estimate

PREDICTAND	FORECAST INTERVAL	PREDICTOR SELECTED	CUMULATIVE REDUCTION OF VARIANCE	STANDARD ERROR OF ESTIMATE
Single Site 1-Min Ave RVR At WRV	+ 5 Min	1. Weighted Average(10)WRV	. 848	. 457
		2. 10-Min Average WRV	. 855	. 447
	+15 Min	1. Weighted Average (10)	. 666	. 716
		2. 1-Min Average RWY	. 684	. 696
	+30 Min	1. Weighted Average(10)WRV	. 516	. 916
		2. 1-Min Average RWY	. 539	. 895
	+60 Min	1. Weighted Average(10)WRV	. 346	1. 159
		2. 1-Min Average RWY	. 364	1. 142
3-Site 1-Min Average RVR	+ 5 Min	1. Weighted Average(10)BED	. 837	. 379
		2. Standard Deviation BED	. 846	. 368
	+15 Min	1. Weighted Average BED	. 666	. 604
		2. 1-Min Average RWY	. 689	. 583
	+30 Min	1. 1-Min Average RWY	. 513	. 809
		2. Weighted Average(10)BED	. 531	. 793
	+60 Min	1. 1-Min Average RWY	. 336	1. 083
		2. Sun Time	. 350	1. 071
Lowest 1-Min RVR Any of 3-Sites over 10-Min* Period	+ 5 Min	1. Lowest RVR Any of 3-Sites	. 893	. 304
		2. 1-Min Average BED	. 918	. 267
	+15 Min	1. Lowest RVR Any of 3-Sites	. 746	. 494
		2. 1-Min Average BED	. 777	. 462

TABLE 3. (continued)

PREDICTAND FORECAST INTERVAL	PREDICTOR SELECTED	CUMULATIVE REDUCTION OF VARIANCE	STANDARD ERROR OF ESTIMATE
+30 Min	1. Weighted Average(3)BED	. 559	. 739
	2. Lowest RVR Any of 3-Sites	. 568	. 731
*Over 5 - Min For 5 - Min Forecast Interval	1. Weighted Average(10)BED	. 341	1. 058
	2. Sun Time	. 356	1. 046

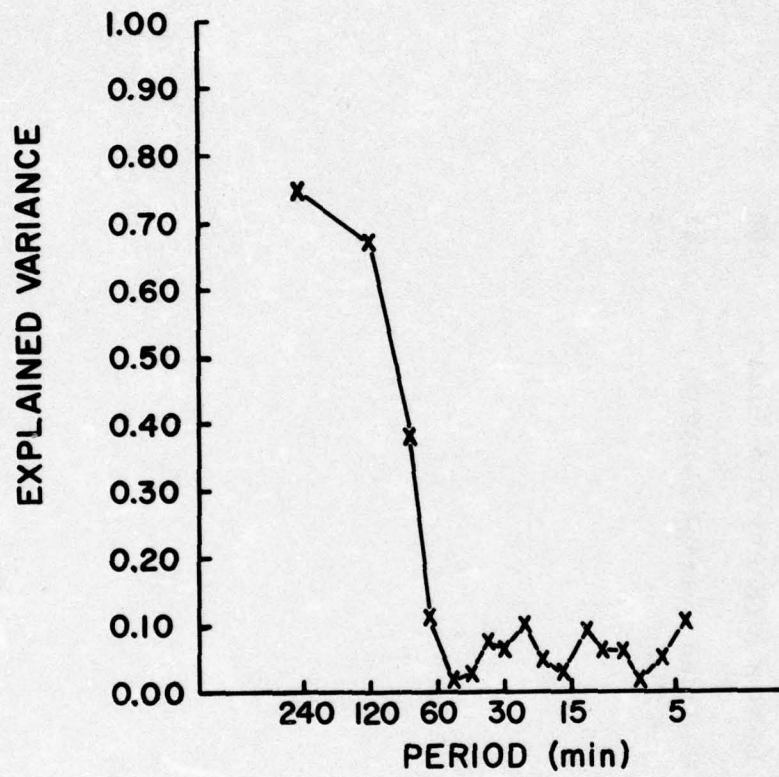


FIGURE 1  
CORRELATION SPECTRUM BETWEEN  
POINT VISIBILITY MEASUREMENTS

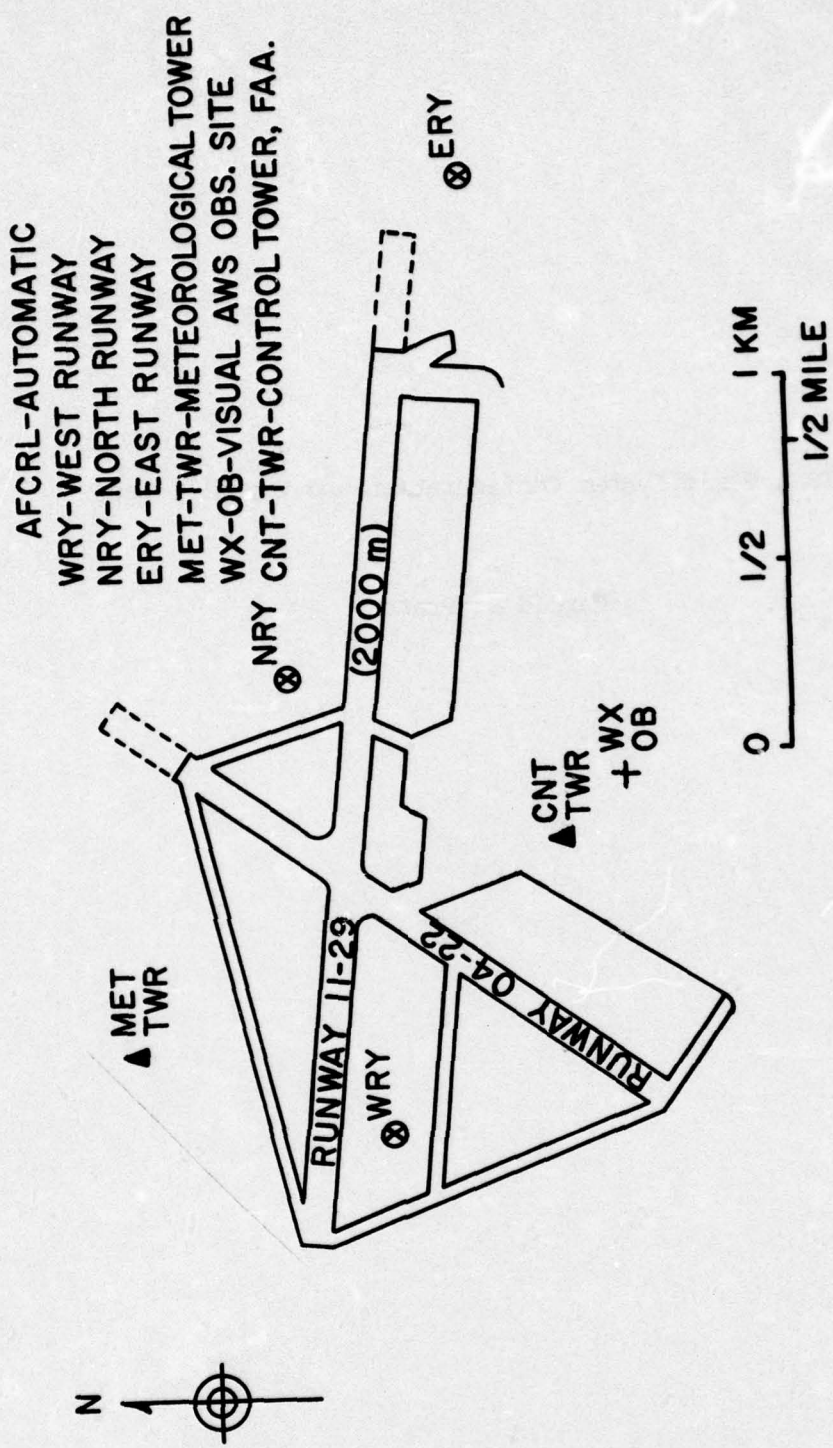


FIGURE 2  
 SCHEMATIC DIAGRAM SHOWING  
 LOCATIONS OF OBSERVATION SITES

**McIDAS: Basic System Configuration and Capabilities**

**Harold J. Pratt**

## 2.1 INTRODUCTION

McIDAS is a real time interactive computer system developed to archive, process, analyze and display meteorological satellite images. The original system was developed at the Space Sciences Engineering Center of the University of Wisconsin. In mid 1974, a copy of a major portion of the system (both hardware and software) was acquired by AFGL. At that time, the system was operational but was still in a relatively early developmental phase. This report discusses the general basic system configuration and its capabilities. Specifics are restricted to improvements and changes made in the system to adapt it for AFGL usage.

## 2.2 McIDAS SYSTEM CONFIGURATION

A functional system diagram of McIDAS is shown in Fig. 1. The SMS/GOES series of synchronous meteorological satellites acquire infrared (IR) and visible earth images using a scanning radiometer. The raw digital data are telemetered to an earth station (Wallops Island, VA) at a high data rate. This information is stretched in time and map gridded. The stretched data are transmitted back to the satellite for retransmission (1687.1 MHz) to other earth receiving stations at a much lower data rate. A NOAA receiving station at Suitland, MD receives the stretched data, sectorizes and processes them and then transmits them over telephone lines on a 2400 Hz carrier. The real time inputs to McIDAS therefore come from two sources, the stretched raw data retransmitted from the satellite and the

sectorized, partially processed data from NOAA, Suitland. The full globe raw data received from the satellite can be archived (digitally) on a video tape recorder or can be fed directly to the McIDAS computer for processing. The sectorized data are archived on standard 9 track magnetic tape or processed directly.

The multiple capabilities of McIDAS are better understood by examining a more detailed block diagram of the system (Fig. 2). The computer is a 24 bit word Harris (Datacraft) 6024/5 medium size computer with 32K of random access memory. Standard peripherals available are a card reader, a line printer, a teletype and two magnetic tape transports. Real time data enter through the antenna system where they are archived on video tape or fed directly to the computer. Sectorized data received over dedicated telephone lines are acquired through a data ingestion module and fed to the computer. The processed digital images are stored on a video disc (250 images) where they can then be recalled and enhanced in black and white or color and displayed on a color monitor. A variety of application programs is available to the operator through a series of simplified keyboard commands. Calculation of wind vectors, generation of animation loops of images and scheduled unattended ingestion of data, are only a few examples of the capability of McIDAS. For a much more complete description of the original McIDAS system, the interested reader is referred to Reference 1.

### 2.3 AFGL McIDAS

Rather than attempt to separate software and hardware changes and

improvements made to the original system, it is more convenient to examine them concurrently in terms of specific applications. An explanation of the various forms the data may be present in the system is also pertinent at this time. As was described earlier, images to be displayed on the monitor are stored on a video disc in analog form. If, in addition to simply displaying the image, the operator also needs to manipulate the image (i. e. , translation, rotation or magnification of the image or analysis of some parameter based on the data), the image must also be accessible to the computer in digital form. This is accomplished by using fixed areas of the digital disc as temporary storage. The digital data are formatted in a fashion similar to the raster of the television monitor, 500 lines by 672 pixels/line. The data word is 8 bits long and therefore will have values between 0 and 255 decimal.

#### 2.3.1 Determination of the value of a point on the displayed image.

As just stated, the image must be present on the digital disc as well as the video disc for processing. Since the monitor has also been provided with a cursor (cursor location is under computer control), it is a relatively simple problem to find the point on the display in terms of the line and pixel numbers. Knowing these coordinates the value of that point can be "looked up" in the digital image.

The format of this command is GD NAREA where NAREA is the number of the temporary digital image storage area on the digital disc.

### 2.3.2 Effective temperature of a point on an IR image

Using the previous program as a basis for determining the "value" of a point in the displayed image, this routine simply relates the data value to the calibration data for the scanning IR radiometer aboard the satellite. In the case of the sectorized data received over the telephone lines, a temperature calibration scale is included with the picture identification as part of the image. This program checks the received calibration scale against expected calibration data and if there is a discrepancy, it informs the operator and calculates a value of effective temperature linearly corrected against the expected calibration. The command is simply GT NAREA.

### 2.3.3 Sectorized ingestion programs

There were two ingestion programs in the original McIDAS system. Both acquired sectorized data via the telephone lines and stored them on the video disc or on 9 track magnetic tape. In the video disc program, the original data are lost. In addition this program was only capable of reading every other line and every second element of an array of 1670 lines by 1200 pixels/lines, thus only part of a picture could be displayed. In addition the starting point was fixed at the first line and first element.

It was found that the ability to read only every other line was due to a speed limitation of the program. By double buffering the input, one line of data is read while the other is transferred to the

digital disc for temporary storage, the speed of the ingestion routine could be increased so that every line could be ingested. In addition the sampling rate of the input data was doubled from 1200 Hz to 2400 Hz, thus doubling the number of pixels/line to 2400. Other features added were a complete choice of starting line and element and line and element increments so the image could be sectorized in any fashion up to the resolution of the input data.

In the next section of this report, unattended schedulers for ingesting data are described. In conjunction with these schedulers several concomitant features were included in the ingestion programs.

The ingestion program normally starts reading when a frame (image) start signal is received. It was found that noise on the input lines could produce false starts. Therefore additional logic and software were added to monitor the input signal. Although it can be changed easily, the criterion used presently is to test and see if the signal is still active for each line of input data. If it has become inactive, the program records this fact and proceeds to look at the next line of data. If the signal has remained low for a period equivalent to 10 lines of data or the signal has flipped on and off 5 times before an image is completed, a decision to abort is made. If greater than 50% of the required lines have been recorded, the picture is retained; otherwise it is deleted.

Provision has also been made to specify a fixed time increment that the program will wait for a frame start. If the time is

exceeded, the program aborts.

A similar program exists for archiving the sectorized data on 9 track - 800 BPI magnetic tape. No options on start line, start element, line increment or element increment are included and the full resolution image is always recorded. A total of four 1670 line by 2400 pixel/line images can be recorded on a standard 10" reel.

The command for loading the image directly to the video disc is:

JB NCHANL NAREA LININC ELMINC LNSTRT ELSTRT TIME

where NCHANL = system ingestion channel code

NAREA = digital disc image storage area

LININC = line increment

ELMINC = element increment

LNSTRT = line start number

ELSTRT = element start number

TIME = interval program is to wait for a frame start

DF NAREA

The command for loading the full sectorized image on magnetic tape is:

RT NCHANL NLINES TTASGN TIME

where NLINES = number of lines/image

TTASGN = tape transport assignment number

These programs will form the basis of routines to be written for the ingestion of raw data directly from the satellite.

#### 2.3.4 Real time ingestion schedulers

Independent schedulers were written for the two previously described ingestion programs. The possibility of the "simultaneous" loading of the tape and video disc was considered but the usefulness of this capability did not warrant the complexity of the programming. Loading of images recorded on magnetic tape to the video disc will be discussed in the following section.

The tape and disc schedulers are very similar. The computer clock and date are used as reference. A start time and start date (of up to 4 days in the future) as well as the interval between images may be selected. The number of images to be recorded may be specified or the program will determine the maximum number that can be recorded on the magnetic tape or loaded on the video disc on the basis of the starting track number of the video disc and its maximum capacity (250). In addition, the number of lines/image can be specified for the tape scheduler.

In the event a frame start has not been found within a specified time interval that would not interfere with the next possible image, or an image has been aborted before completion, the ingestion program is rescheduled for the next possible image (1/2 hour interval). Once a successful image has been acquired, the schedule is then resumed on the basis of the last recorded picture and the operator specified time interval between pictures.

If an image has been aborted, the scheduler takes this into

account. Tape is repositioned to the beginning of the partially recorded image and will be written over. For the video disc, the instruction to write the video disc is simply ignored. Particular care was taken to insure that the scheduler would take away a minimum time from other possible foreground and background processing. The ingestion program is active only a small time (approximately 1 minute) before the expected image. The scheduler itself is placed in a wait mode (periodic checks with the computer clock) and only becomes active a few seconds before the ingestion program.

The command for the video disc scheduler is:

```
VS  MMDDYY  HHMMSS  PICINT  NPIC  STRTRK
    NCHANL  NAREA   LININC  ELMNC  LNSTRT  ELSTRT  TIME
```

where MMDDYY = starting date            month            day            year

HHMMSS = starting time            hour            minute            second

PICINT = image interval in minutes

NPIC = number of images

0 = default = program calculates NPIC

STRTRK = starting track number for the video disc

The remaining parameters have been defined earlier.

The command for the tape scheduler is:

```
TS  MMDDYY  HHMMSS  PICINT  NLINES  NPIC  NCHANL
```

These parameters also have been defined earlier.

### 2.3.5 Transfer of an image recorded on 9 track tape to digital disc

This program reads recorded digital images from a 9 track tape according to starting line, starting element, line increment and element increment options and stores them in a specified temporary digital disc storage area. Images are separated by ends of files. A routine within the program keeps track of file numbers and therefore transfer between files is possible without lengthy rewinding and searching. Once the image has been loaded on the digital disc, a second command (DF NAREA) can be given to load the image on the video disc for display.

The command for reading the image tape is:

TA NFILE NAREA MXR NLINE LININC ELNINC LNSTR ELSTR

where NFILE = tape file number

NAREA = digital disc area

MXR = 3 character multiple command

1st character = R or C

R = rewind tape

C = proceed from where tape  
is presently positioned

2nd character = 0 or 1

0 = top transport

1 = bottom transport

3rd character = 0 to 9

= the maximum number of  
images on the tape

### 2.3.6 Record exact size digital image from magnetic tape to digital disc and vice versa

Since the loading of images from a full resolution tape is time consuming, these routines were written as a method of recording and retrieving images that have already been sectorized by earlier programs.

The SAVE program selects the image on the digital disc and writes it on the tape. Restore is the inverse program. As in the previous description, the program has its own internal file numbering routine for the tape. Rapid access between files is possible without lengthy rewinding and searching.

The SAVE program command is:

```
SA  STARTAR  ENDAR  NFILE   $\frac{R}{C}$   NTAPE
```

where STARTAR = starting digital disc area

ENDAR = ending digital disc area

NFILE = tape file number

R/C = R or C = rewind or continue tape

NTAPE = tape transport number

The RESTORE command is:

```
RA  NPIC  STARTAD  NFILE   $\frac{R}{C}$   NTAPE
```

where NPIC = picture number within each file

### 2.3.7 Special application routines

A series of programs for a specific research project has also

been written. These are summarized here briefly as they are mainly given as examples of the programming flexibility of the system.

Data for the project are received in the form of images in a north polar stereographic projection recorded on 9 track tape. IR and visible data were intermixed and record lengths were unique. A variation of the program discussed in 2.3.5 was developed that permitted a rapid display of the data on McIDAS. Routines were also written to average images, remove an image from an image average, reverse images left to right and top to bottom. A program, which is nearly complete, permits an image to be transferred from one map projection to another and then displayed and compared quantitatively. Rotation and translation of the images are also included.

#### 2.4 Summary

This report has been concerned primarily with examples of McIDAS applications programs. Numerous hardware and system software modifications have also been made but would be of primary interest only to one involved in similar problems. The main point to be made is that McIDAS is an extremely powerful and flexible system. It can easily (usually) be modified for use in a variety of image problems. The video tape archiving (mass storage) and the image color enhancement schemes were only briefly mentioned. Further study and expansion of these capabilities are planned for the near future.

## REFERENCES

- 1 **Man-Computer Interactive Data Access System (McIDAS), Final Report, 24 July 1973, University of Wisconsin, Space Science and Engineering Center, Madison, Wisconsin; prepared for Goddard Space Flight Center, Greenbelt, Maryland.**

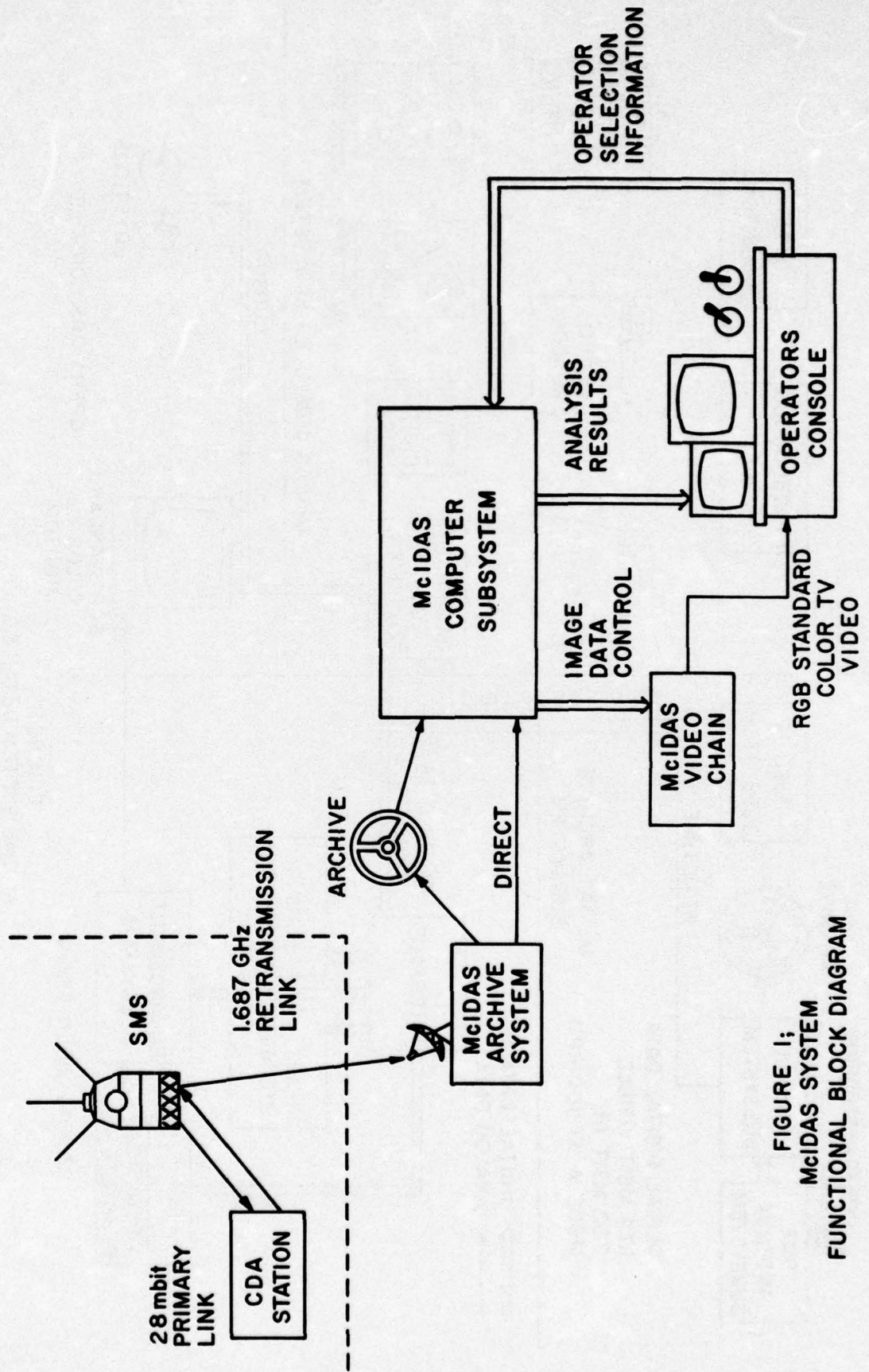


FIGURE 1;  
McIDAS SYSTEM  
FUNCTIONAL BLOCK DIAGRAM

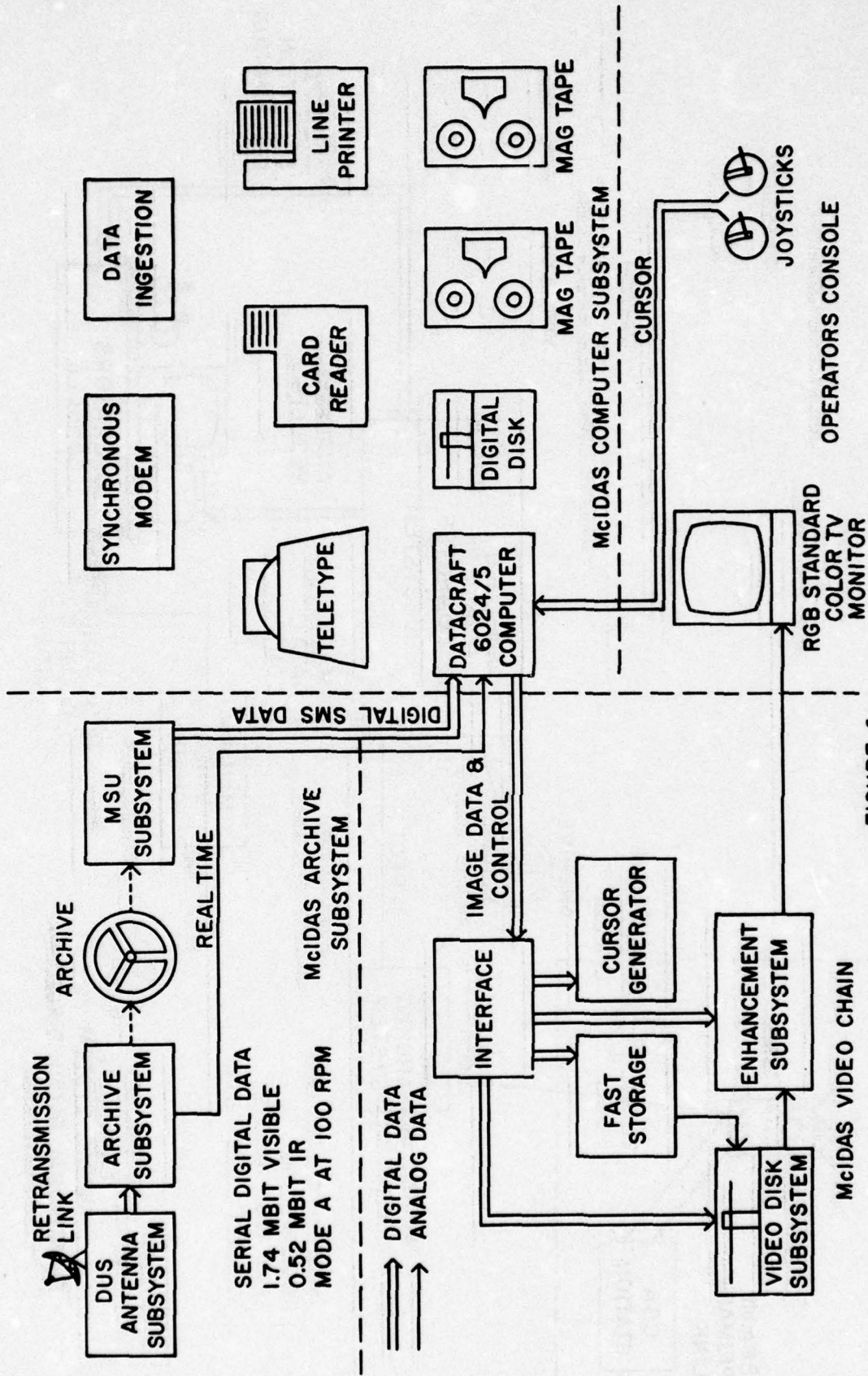


FIGURE 2.1  
 McIDAS SYSTEM DETAILED  
 FUNCTIONAL BLOCK DIAGRAM

**Numerical Schemes for Radioactive Change of Surface Air Temperature**

**Roy Glasser**

### 3.0 Numerical Schemes for Radiative Change of Surface Air Temperature

Roy Glasser

#### 3.1 Introduction

The Air Force Global Weather Central Boundary Layer Model (AFGWC-BLM) assumes the radiative change of the surface temperature to be given by

$$\left(\frac{\partial T}{\partial t}\right)_R = C \left(\frac{\partial T}{\partial t}\right)_C \quad (1)$$

The terms  $\left(\frac{\partial T}{\partial t}\right)_R$  and  $\left(\frac{\partial T}{\partial t}\right)_C$  represent the time rates of change of the air temperature at the surface due respectively to radiation and climatology.

The constant of proportion  $C$  is a function of cloud cover. Determined primarily by the types and amounts of clouds in the free atmosphere, this constant is modified by the clouds present in the planetary boundary layer.

The climatological surface air temperature,  $T_C$ , is approximated in the current AFGWC-BLM by

$$T_C(t) = -A(\phi, \tau) \sin\left[\frac{(t+3)\pi}{12}\right] \quad (2)$$

in which  $t$  is the time of the day in hours.  $A(\phi, \tau)$  is a function of the latitude of the point,  $\phi$ , and of the time of the year,  $\tau$ , that are under consideration. This function is determined from climatology for each grid point and for each month of the year.

### 3.2 Numerical Schemes

When the surface air temperature,  $T_C(t)$ , is given in accordance with (2), the time rate of change  $\left(\frac{\partial T}{\partial t}\right)_C$  may be approximated by either of the following finite-difference formulas:

(i) backward difference

$$\frac{T(t) - T(t - \Delta t)}{\Delta t} \quad (3a)$$

(ii) forward difference

$$\frac{T(t + \Delta t) - T(t)}{\Delta t} \quad (3b)$$

Expansion of (3a) and (3b) by Taylor's series shows that they are both of the first order of accuracy. The current AFGWC-BLM employs formula (3a). It is of interest to determine whether formula (3b) produces any significant difference in the forecast accuracy of the model.

### 3.3 Method of Experiment

Since the AFGWC-BLM is a highly complicated model of the planetary boundary layer, in which a number of non-linear processes take place, the method of twin experiments was considered to be the most effective investigative technique. This method utilizes twin models which are identical in all respects except for the feature under study. These models are run under identical conditions, i. e. on identical input data. If the difference between the twins, which is the feature under study, does not drastically change the nature of the models, the difference in the results between the

twins may be regarded as the response of the model as a whole to the difference introduced. Analyses of the results of such runs under a number of different conditions provide further insight into the magnitude of the response.

Confidence in inferences drawn from such analyses are enhanced if these inferences remain valid when analysis is made of another pair of twins which has the same difference between them as does the first pair, but is slightly different in other respects.

Based on the preceding considerations, the following series of parallel twin experiments was designed and carried out. Two pairs of twin models of the AFGWC-BLM genre (see Figure 1) were employed. Models AB and AF and models BB and BF differ from each other in the manner in which the calculated values of the temperature are stored in the memory of the computer. This difference is believed to be unrelated to the question at hand, i. e., the numerical scheme used to determine the change in the surface air temperature. Models AB and BB use the backward difference formula (3a), while models AF and BF use the forward difference formula (3b), for the time rate of change of the climatological surface air temperature.

Each of the four models was run under the same set of different conditions to produce 12-hour and 24-hour forecasts for the entire planetary boundary layer in an area of approximately 10,000,000 km<sup>2</sup>. The sample considered in this study consisted of nine cases of 12-hour forecasts over

the daytime half of a day, eight cases of 12-hour forecasts over the nighttime half of a day, and nine cases of 24-hour forecasts which began at 1200Z.

### 3.4 Analysis - Theory

Since our primary interest is in the forecast accuracies of the models, analyses were conducted with respect to forecast errors. These errors are defined as differences between predicted and observed values. Although the models predict temperature, wind, and humidity, the analyses were limited to a consideration of the air temperature alone, since it was felt that this quantity would be most directly affected by the difference.

The air temperature forecast error for each model was characterized at selected levels in the vertical at a given time. This was accomplished by two statistical parameters in the physical space and one vector of seven components in the wave-number space. These parameters in the physical space are the bias,  $m$ , and the standard deviation,  $s$ , of the forecast errors, defined respectively by

$$m = \frac{1}{N} \sum_{i=1}^N e_i \quad (4a)$$

$$S^2 = \frac{1}{N} \sum_{i=1}^N e_i^2 - m^2, \text{ for } S \geq 0 \quad (4b)$$

where  $N$  is the total number of grid points on each level. The seven vector components in the wave-number space,  $\{ E_i, i=1, 2, \dots, 7 \}$ , where

$i$  is the cell index, are the fractions of energy in seven mutually exclusive and collectively exhaustive cells in the wave-number space. Cell ordering is arranged so that the representative wavelength of a cell becomes shorter as the cell index becomes larger. The vector represents the relative distribution of energy of the difference of errors.

### 3.5 Analysis - Application and Discussion

The entire depth of the planetary boundary layer was represented by four levels for the purposes of this analysis. The four selected were level 0 at the surface, level 3 at 300 meters above ground (AG), level 5 at 900 m AG, and level 7 at 1600 m AG.

The statistical parameters in the physical space are summarized by differencing the appropriate forecast model errors. Thus, differences  $D_1$  and  $D_2$  are defined by

$$D_1 = E_{AF} - E_{AB}$$

$$D_2 = E_{BF} - E_{BB}$$

where  $E_{AF}$ , for example, is the forecast error of model AF. Table 1 presents a summary of these differences for the 12-hour temperature forecast. The group means (M) and standard deviations (S) are calculated for each of the parameters  $m$  and  $s$  to obtain the entries into the table. A high degree of statistical similarity between  $D_1$  and  $D_2$  in both the day and night groups is seen in the table. During the day both  $D_1$  and  $D_2$  increase

monotonically with height from  $-0.5^{\circ}\text{K}$  at the surface to  $-0.1^{\circ}\text{K}$  at the top. There seems also to be a statistically significant difference of  $0.1^{\circ}\text{K}$  in the bias between  $D_1$  and  $D_2$  in the middle of the boundary layer at this time. At night, on the other hand, there is very little difference between the two at all levels. Both  $D_1$  and  $D_2$  have a bias of  $0.4^{\circ}\text{K}$  at the surface and no bias at higher levels.

We thus note that the effect of the difference between the finite difference formulas is greatest at the surface and diminishes with height during both the day and night. The more intense daytime turbulent heat transfer is probably the cause of the surface change being reflected more at high levels during daytime than at nighttime. We also note that the effect at the surface at night is opposite to that at daytime. This may be due to the characteristics of the difference between the real and approximate temperatures.

Figures 2.1 through 2.4 present the statistics of the energy distribution for  $D_1$  and  $D_2$ . Two salient features to be noted in these figures are (1) the similarity of the profiles between  $D_1$  and  $D_2$  in both the day and night groups, and (2) most of the energy of the differences is found in short waves both during the day and at night, except for that at the surface in daytime.

Tables 2.1 and 2.2 present the statistics of the forecast errors of the individual models for the day and night groups, respectively. They represent the effect of the difference between the difference formulas

observed as the response of the total model. There is little difference in the standard deviation between Models AB and AF or between Models BB and BF. The only significant difference is found in the group means of the biases which are none other than the group means of the averages of  $D_1$  and  $D_2$ .

Table 3 lists the root-mean-squares (rms) of the forecast error of the four models at four levels for the day and night groups of the 12-hour forecasts. It is apparent that comparatively larger and uniform spatial standard deviations, i. e., entries (s, M), found in Tables 2.1 and 2.2 dominate the composition of the rms forecast errors to make these indistinguishable between Models AB and AF and between Models BB and BF.

Tables 4, 5, and 6 and Figures 3.1 and 3.2 summarize the statistics of the forecast errors for the 24-hour forecasts. Comparisons of Table 4 with Table 1 and of Table 5 with Tables 2.1 and 2.2 show that the error of a 24-hour forecast is not a sum of the errors of two 12-hour forecasts in the same period. In general, both the spatial standard deviation and the group standard deviation are greater for the 24-hour forecasts than for the 12-hour forecasts. There is less difference among different levels in the distribution of the energy of the difference in the 24-hour forecasts. In addition, a large fraction of energy found in the long waves at the surface in the day group of the 12-hour forecasts is completely missing in the 24-hour forecasts.

Comparison of Model AF with AB and Model BF with BB in Tables 5

and 6 leads to observations similar to those noted for Tables 2.1, 2.2, and 3.

### 3.6 Conclusions

The difference in the finite-difference formulas for the time rate of change in the surface air temperature does not produce any statistically significant change in the forecast accuracy for both 12-hour and 24-hour forecasts.

FORECAST PERIOD		LEVEL											
		0		3		5		7					
		m	s	m	s	m	s	m	s				
Day	D1	M	-.51	.48	-.26	.39	-.21	.34	-.09	.28			
		S	.04	.04	.03	.02	.02	.02	.03	.02			
	D2	M	-.52	.46	-.17	.43	-.14	.34	-.07	.23			
		S	.04	.04	.05	.02	.02	.02	.02	.09			
Night	D1	M	.40	.70	-.01	.60	-.01	.33	-.01	.27			
		S	.04	.18	.05	.05	.02	.02	.01	.03			
	D2	M	.41	.75	.00	.60	-.01	.38	-.03	.30			
		S	.06	.27	.04	.08	.02	.07	.02	.10			

Table 1. Statistics of Differences of Forecast Errors  
12-hr. T (°K) - Forecasts

		LEVEL											
		0		3		5		7					
		m	s	m	s	m	s	m	s	m	s	m	s
MODEL	AB	M	-0.66	3.59	-0.70	3.62	-1.38	3.47	-0.38	3.34	M	-0.66	3.59
		S	.47	.36	.55	.38	.62	.31	.41	.23	S	.47	.36
MODEL	AF	M	-1.17	3.49	-0.96	3.53	-1.59	3.38	-0.48	3.31	M	-1.17	3.49
		S	.48	.37	.55	.39	.62	.32	.38	.24	S	.48	.37
MODEL	BB	M	-0.51	3.53	0.25	3.56	-0.02	3.24	1.14	3.30	M	-0.51	3.53
		S	.46	.35	.56	.35	.61	.29	.43	.21	S	.46	.35
MODEL	BF	M	-1.03	3.44	0.07	3.51	-0.16	3.19	1.08	3.28	M	-1.03	3.44
		S	.46	.37	.56	.34	.62	.29	.43	.21	S	.46	.37

Table 2.1 Means and Standard Deviations of Forecast Errors

12-hr. T (°K) - Forecasts Day

		LEVEL											
		0		3		5		7					
		m	s	m	s	m	s	m	s	m	s	m	s
MODEL	AB	M	.82	3.02	.63	2.96	.41	2.82	.76	3.02			
		S	.23	.36	.60	.35	.38	.30	.25	.36			
MODEL	AF	M	1.22	2.95	.62	2.93	.40	2.81	.75	3.02			
		S	.23	.37	.57	.34	.38	.28	.25	.36			
MODEL	BB	M	1.04	3.08	3.56	3.27	2.75	2.97	2.64	3.23			
		S	.27	.38	.60	.42	.44	.32	.23	.34			
MODEL	BF	M	1.45	3.00	3.56	3.27	2.74	2.95	2.61	3.21			
		S	.25	.33	.60	.42	.43	.33	.23	.33			

Table 2.2 Means and Standard Deviations of Forecast Errors  
12-hr. T (°K) - Forecasts Night

		LEVEL											
		0		3		5		7					
		DAY	NIGHT	DAY	NIGHT	DAY	NIGHT	DAY	NIGHT	DAY	NIGHT	DAY	NIGHT
MODEL	AB	M	3.67	3.14	3.73	3.07	3.77	2.86	3.38	3.12			
		S	.38	.34	.41	.45	.39	.33	.21	.36			
MODEL	AF	M	3.71	3.21	3.69	3.04	3.79	2.86	3.37	3.12			
		S	.42	.34	.44	.42	.41	.32	.22	.36			
MODEL	BB	M	3.61	3.26	3.62	4.85	3.30	4.05	3.51	4.17			
		S	.42	.35	.33	.65	.28	.45	.30	.35			
MODEL	BF	M	3.61	3.34	3.55	4.84	3.25	4.04	3.47	4.14			
		S	.41	.30	.33	.65	.28	.45	.31	.34			

Table 3. Root-mean-square Forecast Error  
12-hr. T (°K) - Forecasts

		LEVEL											
		0		3		5		7					
		m	s	m	s	m	s	m	s	m	s		
D <sub>1</sub>	M	.10	1.05	-.28	.99	-.19	.56	-.14	.45				
	S	.07	.19	.06	.10	.04	.06	.03	.02				
D <sub>2</sub>	M	.07	1.34	-.21	1.01	-.13	.63	-.08	.54				
	S	.08	.25	.06	.10	.08	.07	.05	.04				

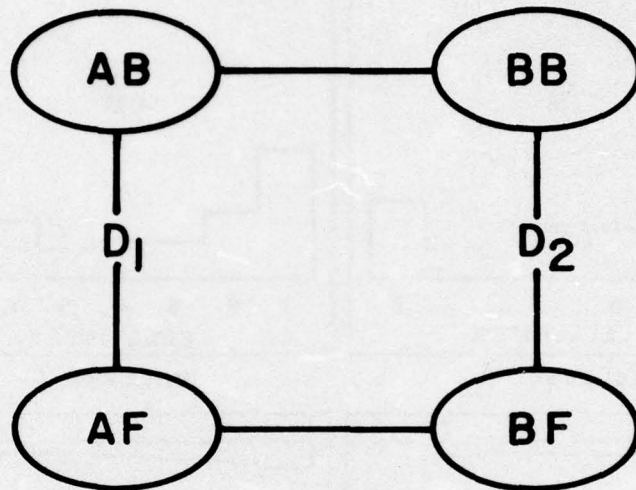
Table 4. Statistics of Differences of Forecast Errors  
24-hr. T (°K) - Forecasts Day Group

		LEVEL											
		0		3		5		7					
		m	s	m	s	m	s	m	s	m	s	m	s
MODEL	AB	M	.39	3.45	.62	3.54	-1.11	3.78	.16	3.99			
		S	.82	.50	.75	.37	.43	.58	.40				
MODEL	AF	M	.49	3.41	.33	3.51	-.30	3.71	-.00	3.98			
		S	.81	.51	.75	.35	.44	.58	.39				
MODEL	BB	M	.64	3.36	4.44	3.89	3.34	3.81	3.37	4.11			
		S	.83	.54	.75	.33	.37	.59	.36				
MODEL	BF	M	.71	3.36	4.22	3.85	3.20	3.75	3.29	4.12			
		S	.79	.48	.72	.36	.37	.61	.35				

Table 5. Means and Standard Deviations of Forecast Errors  
24-hr. T (°K) - Forecasts Day Group

		LEVEL				
		0	3	5	7	
MODEL	AB	M	3.56	3.67	3.85	4.03
		S	.47	.27	.41	.40
MODEL	AF	M	3.54	3.60	3.78	4.02
		S	.48	.30	.45	.39
MODEL	BB	M	3.51	5.93	5.10	5.33
		S	.56	.50	.42	.49
MODEL	BF	M	3.51	5.75	4.97	5.29
		S	.48	.46	.42	.50

Table 6. Root-mean-square Forecast Error  
24-hr. T ( $^{\circ}$ k) - Forecasts Day Group



A SCHEMATIC DIAGRAM OF  
TWIN EXPERIMENTS

FIGURE 1

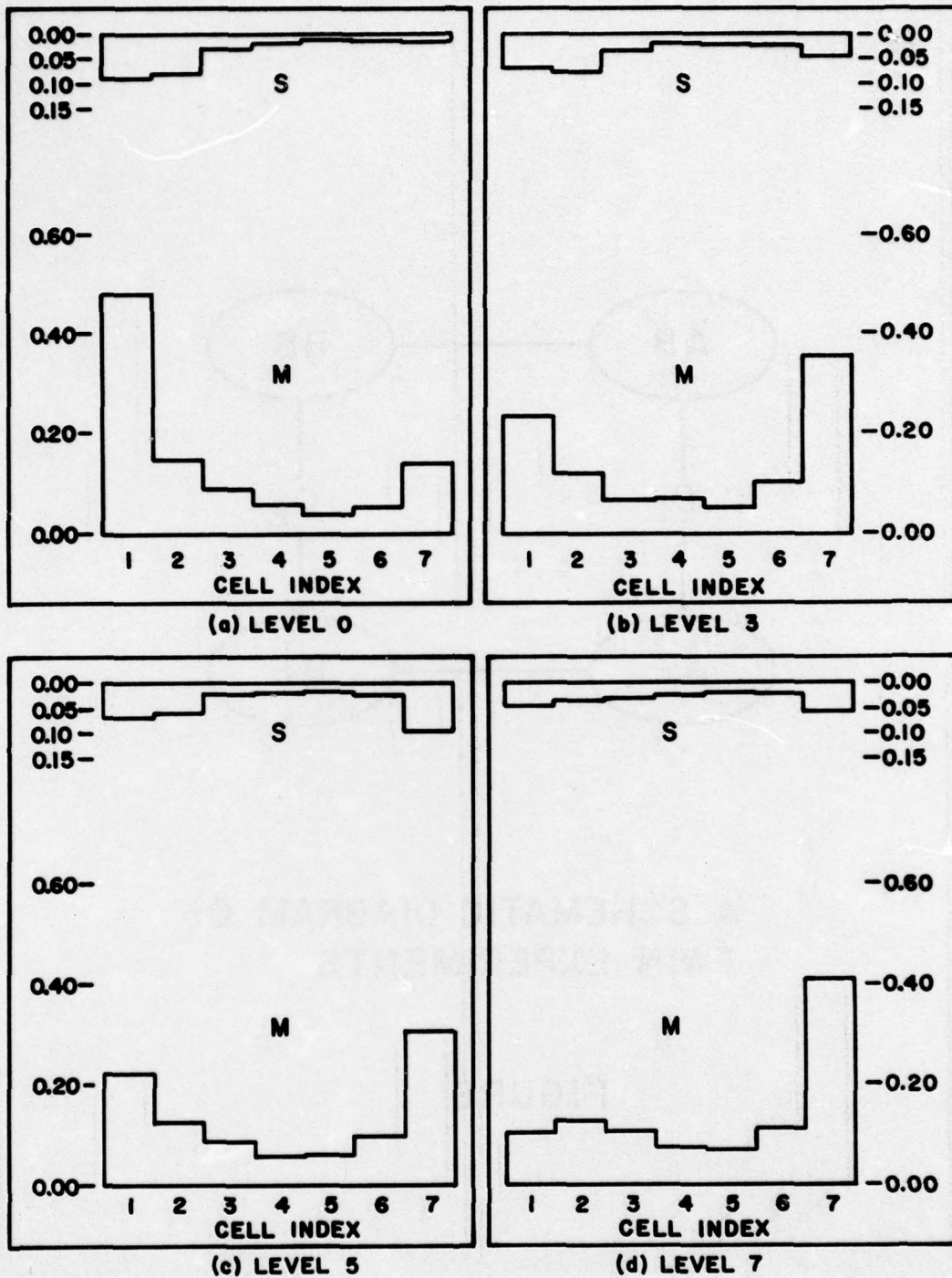


FIGURE 2.1 ENERGY DISTRIBUTION OF  $D_1$   
12-HR T-FORECAST DURING THE DAY

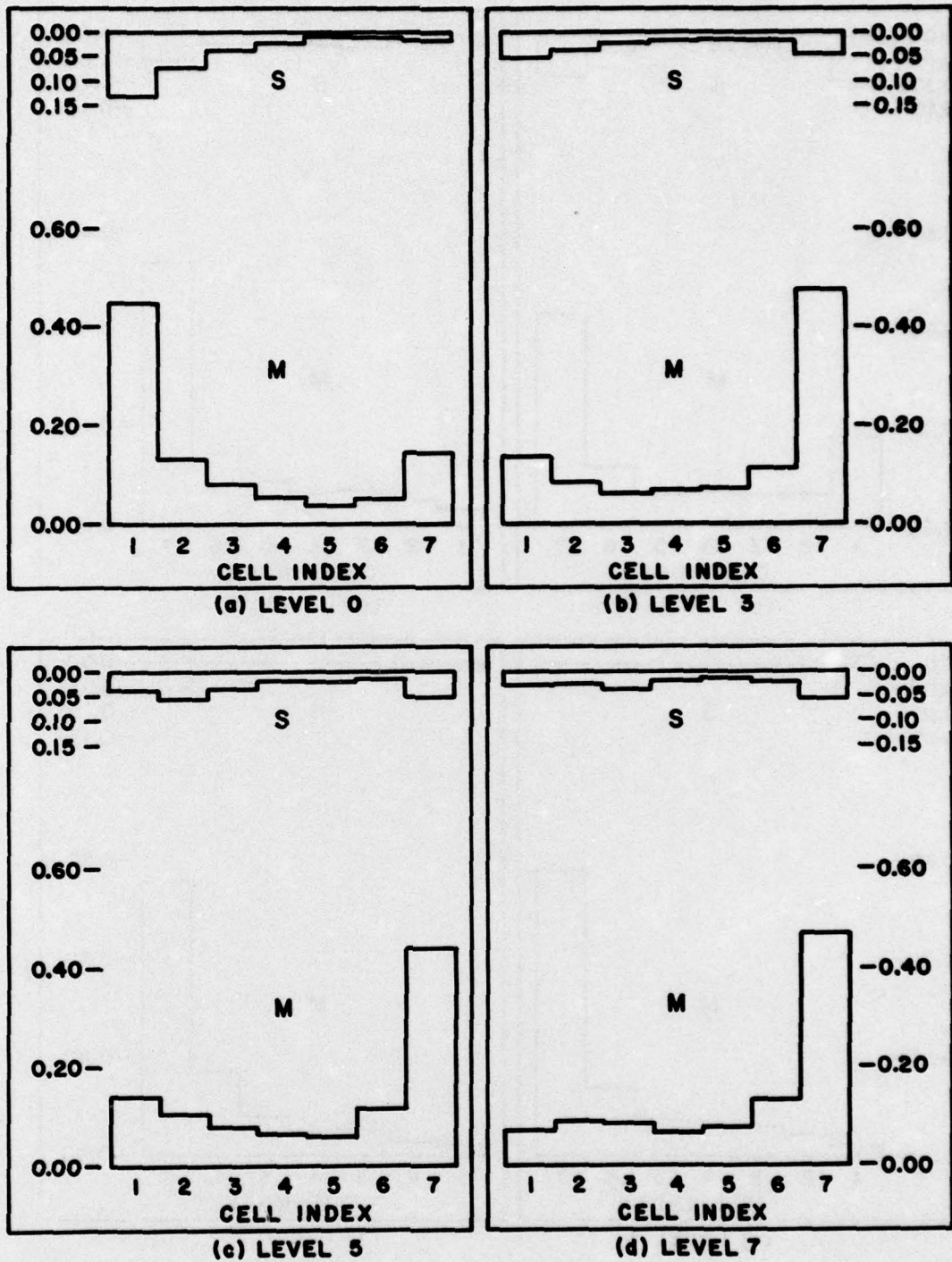


FIGURE 2.2 ENERGY DISTRIBUTION OF  $D_2$   
12-HR T-FORECAST DURING THE DAY

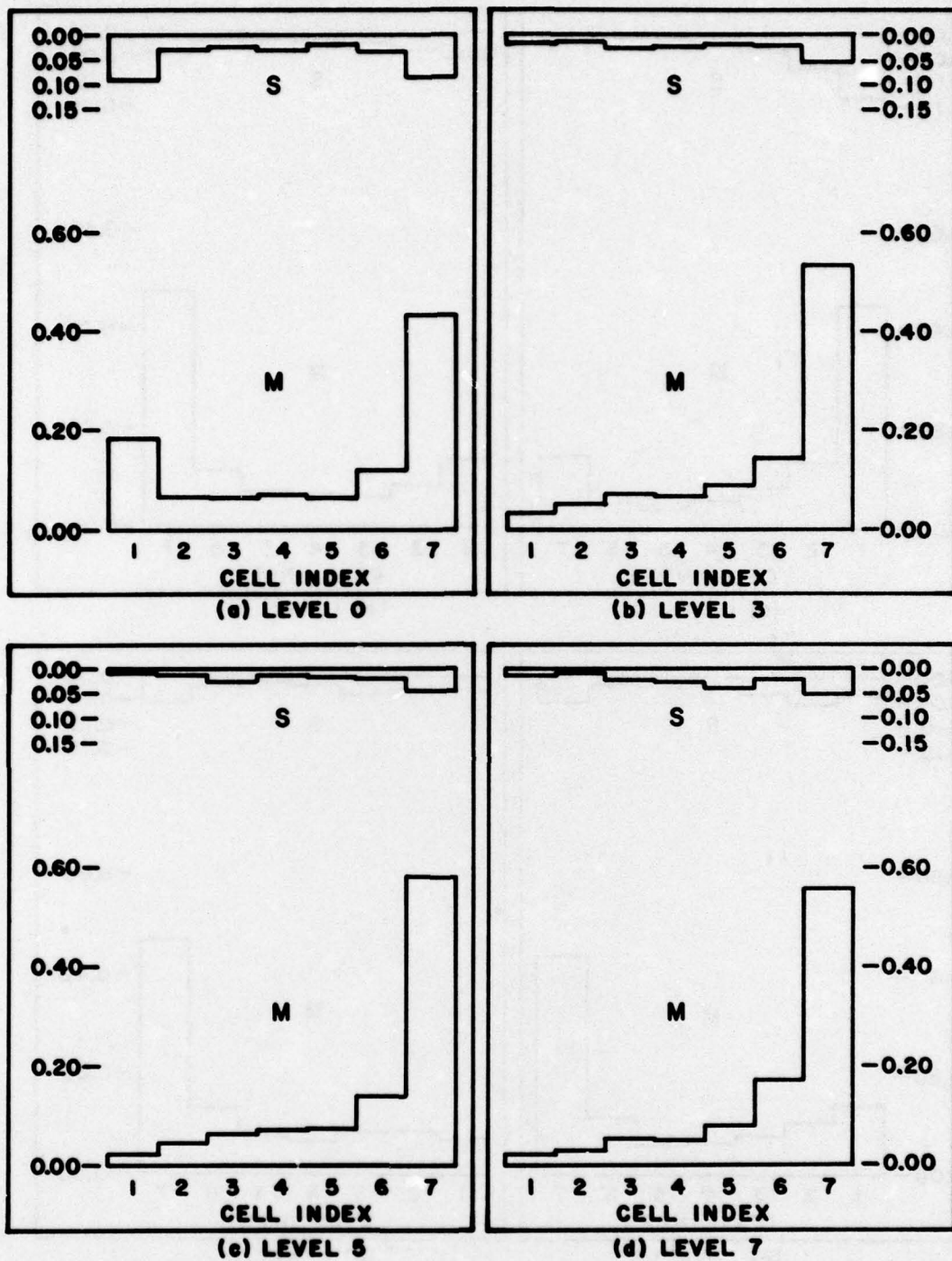


FIGURE 2.3 ENERGY DISTRIBUTION OF  $D_1$   
12-HR T-FORECAST DURING THE NIGHT

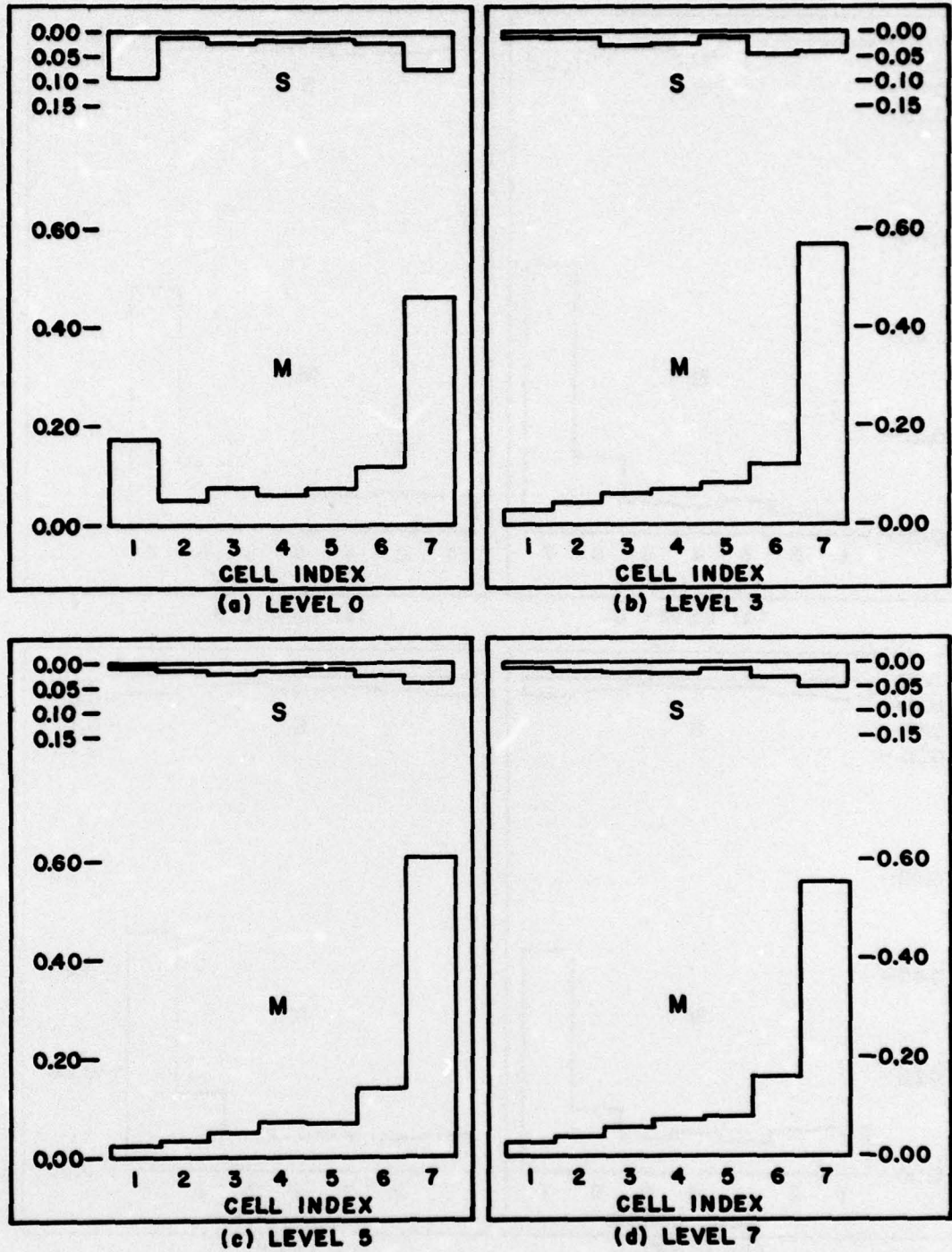


FIGURE 2.4 ENERGY DISTRIBUTION OF  $D_2$   
12-HR T-FORECAST DURING THE NIGHT

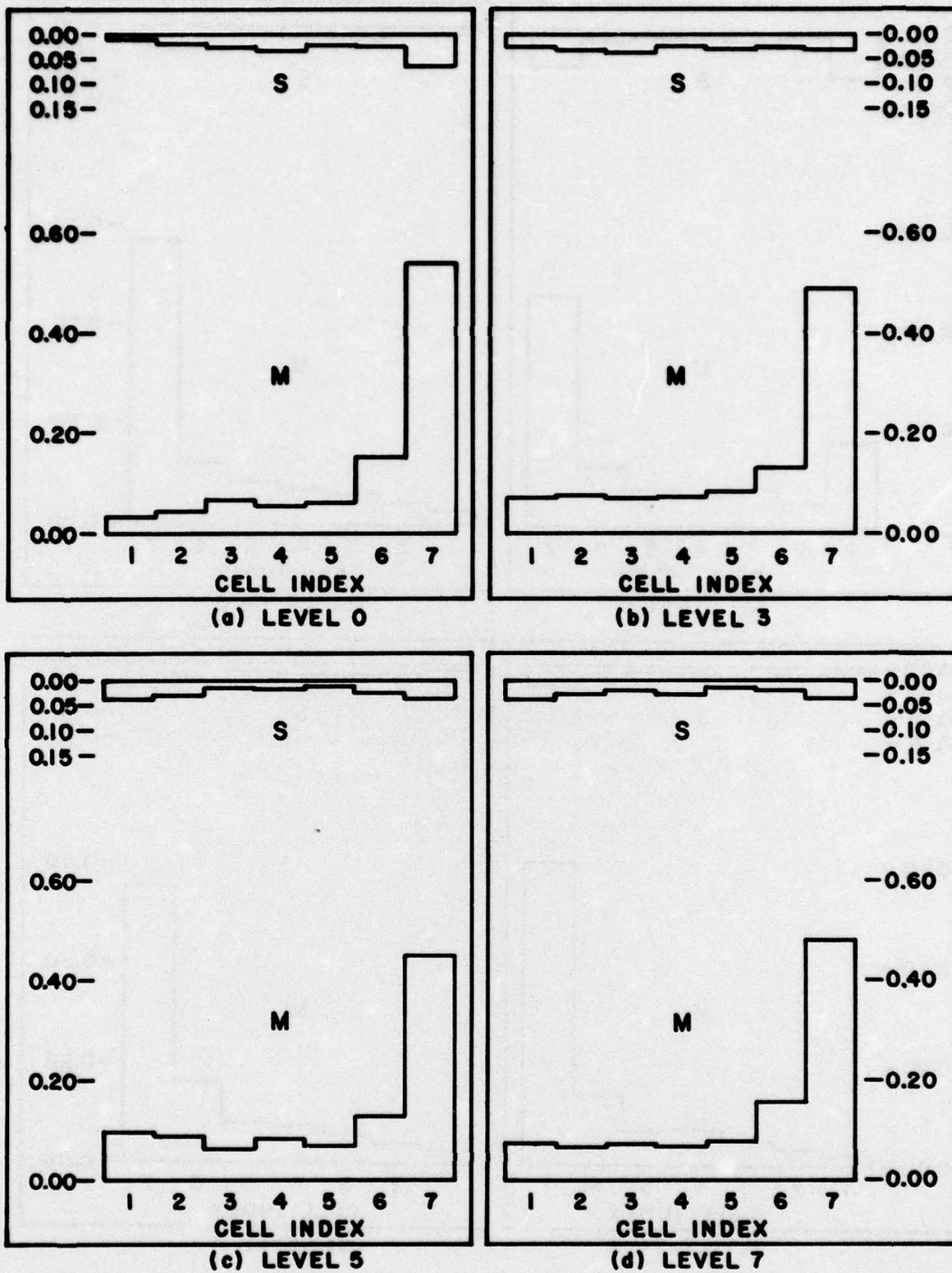


FIGURE 3.1 ENERGY DISTRIBUTION OF  $D_1$   
24-HR T-FORECAST DURING THE DAY

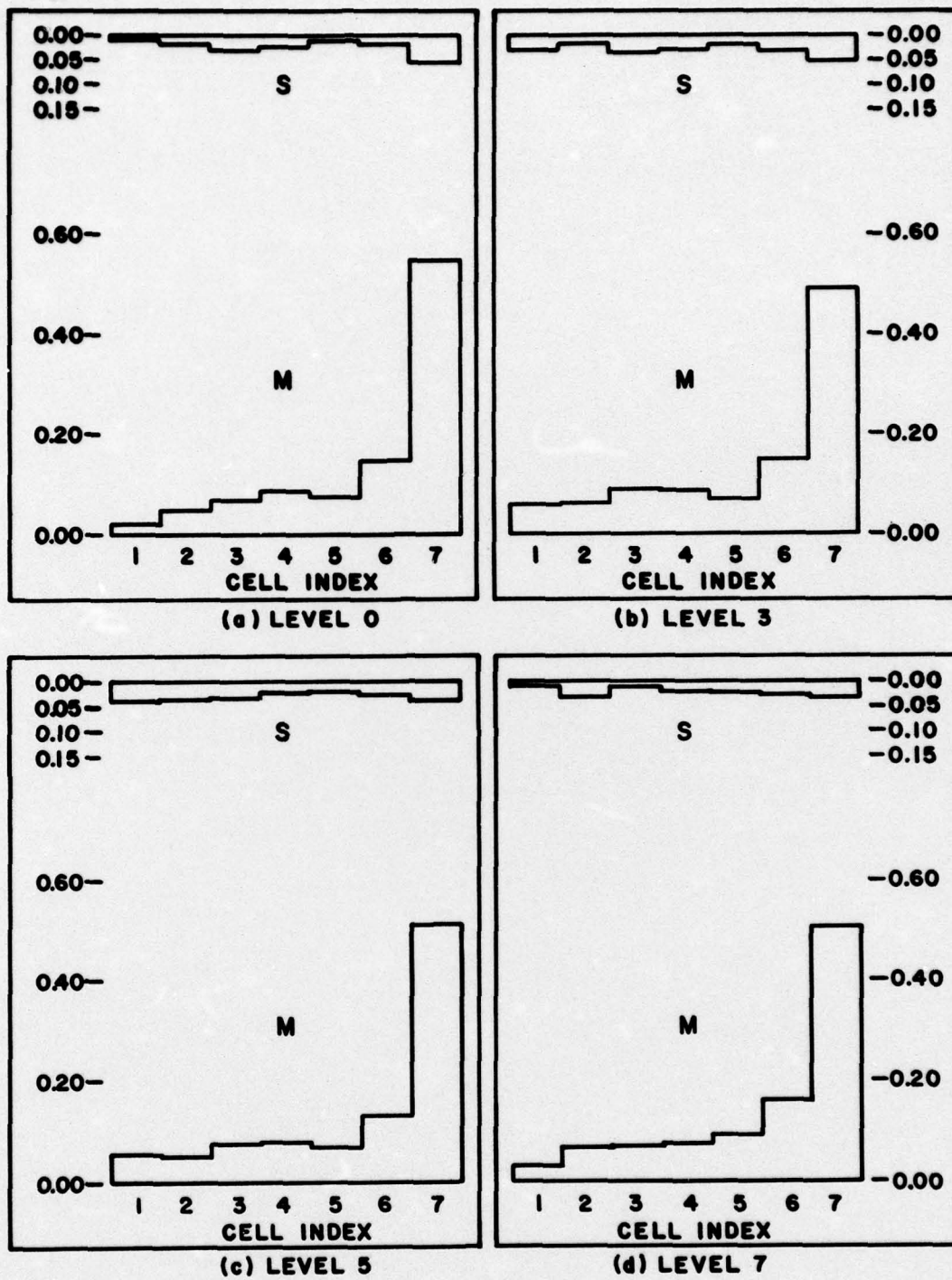


FIGURE 3.2 ENERGY DISTRIBUTION OF  $D_2$   
24-HR T-FORECAST DURING THE DAY